A Microwave Circuit Electric Field Imager

Thomas P. Budka, Student Member IEEE, and Gabriel M. Rebeiz, Senior Member IEEE

NASA Center for Space Terahertz Technology at The University of Michigan
Electrical Engineering and Computer Science Department
Ann Arbor, MI 48109-2122 USA

Abstract

We report on the theory of operation and the experimental results obtained from an electric field imaging system that employs the method of modulated scattering. The system is low cost and is capable of mapping the normal and tangential electric field magnitude and electrical phase delay at each position within 5 μm above a microwave circuit in the frequency range of 0.5 GHz to 18 GHz. The electric field probes are fabricated on a very thin quartz substrate. The measured images of the normal and tangential electric fields over microstrip and coplanar waveguide transmission lines are presented and agree well with theory.

Introduction

Both active and passive probes yield important S-parameters necessary for circuit design but fail to describe the internal operation of devices contained within a MMIC. The mapping of the electromagnetic fields above a MMIC can be of great importance in detecting field magnitudes, electric field direction, phase information, substrate modes, circuit radiation, and device to device interactions. Currently, electromagnetic field mapping is possible with electro-optic sampling[1]-[4], photoemission sampling [5], electron-beam sampling [6], scanning force microscopy [7]-[9] and modulated scattering [10]-[15]. The first three methods are generally time domain methods while the latter two techniques are frequency domain methods.

The modulated scattering technique was developed by several groups in 1955 (Richmond [10], Cullen et al. [11] and Justice et al. [12]). A small dipole with a diode mounted at the center of the dipole arms is placed in the near field of an antenna or circuit of interest. By modulating the bias of the diode at a frequency much lower than the radio frequency (RF), a modulated scattered RF signal would return to the transmitter [10]. The strength and phase of this modulated signal is directly proportional to the electric field intercepted at the position of the dipole probe [10].

Zürcher expanded this technique to probe the tangential near fields over microstrip circuits (patch antennas and hybrid couplers) at frequencies centered around 1.8 GHz [13]. However, he used relatively large probes (9 mm) which limited his spatial resolution [14]. In this paper a coaxial modulated scattering experiment which is optimized for high frequency operation using miniature probe scatterers is presented. The system can be used to simultaneously detect normal and tangential electric fields and the net electrical phase delay within a microwave circuit and is extremely useful for MMIC diagnostics. The system currently works from 0.5 GHz to 18 GHz and can easily be extended for operation below 0.5 GHz and up to 60 GHz using a coaxially based system.

Experiment

A dipole and a monopole of approximately 1/20th of the smallest operating RF wavelength of the microwave circuit under test are used as modulating scatterers. A low resistance, low capacitance diode is mounted on a transmission line that directly feeds the scattering antenna. As the probe containing these scatterers moves across the device under test (DUT), a scattered reflected and transmitted signal is detected by a quadrature mixer. Figure 1 displays the near field detection experiment.

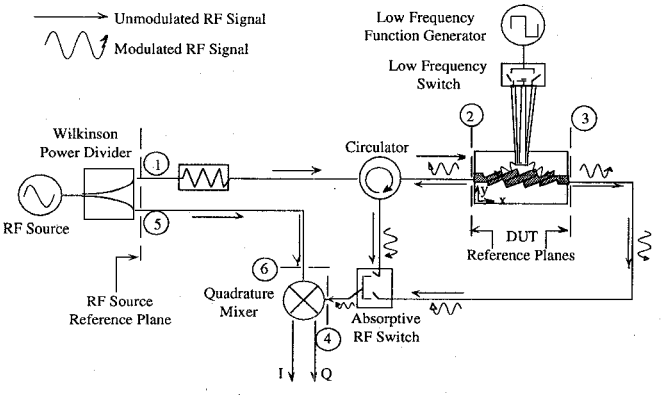

Figure 1. The monolithic microwave integrated circuit electric field imaging experiment using the technique of modulated scattering.

To detect the scattered reflected signal at the input port, the reflected signal is diverted to a wideband homodyne quadrature mixer by a wideband circulator. The in-phase and quadrature signals are then detected with a lock-in amplifier. Through the use of an absorptive RF switch, the transmitted signal magnitude and phase can also be detected from any number output ports. The scattering probes are mounted on a computer controlled submicron translational stage. By scanning the probe over a region of interest in close proximity to the DUT, a complete two dimensional electric field magnitude image and net electrical phase delay image is collected and stored on the computer. Proximity of the dipole or monopole with the DUT and size of the dipole or monopole also determines the electric field resolution of the probe and the strength of the interaction.

CH3577-4/95/0000-1139$01.00 © 1995 IEEE

Figure 2 shows the design of the dipole and monopole scatterers. The probes are fabricated on 125 μm thick low loss quartz (Dynasil 4000 from Accumet). Chrome resistive bias lines are used to absorb any RF fields that may propagate along the bias lines and also serve as current limiters to protect the diodes. These lines have a typical resistance of 100 Ω/mm. Commercially available low cost diodes are then silver epoxied between the dipole arms. For the monopole scatterer, two diodes are placed between the CPW ground planes and the center conductor. The diodes used are beam lead Metelics Corporation low barrier Schottky diodes (component #MSS30-154 B10 and B20) and the modulated bias current is between 0 mA and 3 mA. The diode has a 3 Ω series resistance, 0.25 pF junction capacitance and a 240 GHz cutoff frequency. These diodes are expected to operate up to 60 GHz without encountering any problems with parasitics. The probes are fabricated using standard photolithographic techniques with 1.0 μm thick gold. The monopole and dipole arms are both 100 μm long and it was found that these probes have 40 dB dynamic range.

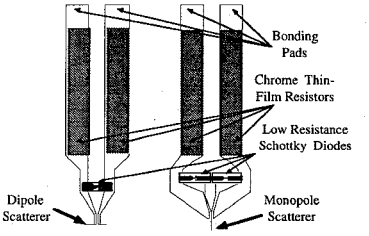

Figure 2. The near field scattering probes. The dipole probe is used for scattering the tangential electric field, and the monopole probe is used for scattering the electric field normal to the MMIC under test.

Theory of Operation

All numerical subscripts for losses and electrical phase delays in this section refer to the numbered points labeled in figure 1. The DUT is chosen to lie in the x-y plane at a height of z=0. If the height of the probe above the DUT is much smaller than a free space wavelength, then we can neglect the phase shift dependence on z. In addition if the height of the probe is constant across the circuit, the phase delay's dependence on z is constant over the entire circuit. The scattered field at the point (x,y,z) will be directly related to the true electric field through the following relationship [10]: $\vec{E}_s(x,y,z) = A(x,y,z)\,\vec{E}(x,y,z)$. The form of the outputs of the quadrature mixer of the modulated signal from the input port is given by:

$$I_r = L_{21}L_{42}L_M L_r(x,y)\,A(x,y,z)\sin(\phi_o - \alpha_i(x,y) - \alpha_r(x,y))$$
$$Q_r = L_{21}L_{42}L_M L_r(x,y)\,A(x,y,z)\cos(\phi_o - \alpha_i(x,y) - \alpha_r(x,y)) \quad \text{(EQ 1)}$$

Where $\phi_o = \phi_{65} - \phi_{21} - \phi_{42} - \alpha_s$ is the sum of the electrical phase delays of the RF signal between the numbered points from figure 1 including a phase delay, α_s, of the scattered signal. For a specific operating frequency, L_{21} and L_{42} are the losses of the RF signal between the numbered points from figure 1. The quadrature mixer conversion loss is given by L_M and $L_r(x,y)$ is the positionally dependent loss the scattered signal encounters when travelling from the probe to the input port of the DUT. The positionally dependent electrical phase delays of the electric field at the point of interest with point 2 being the reference plane are given by $\alpha_i(x,y)$ and $\alpha_r(x,y)$ where $\alpha_i(x,y)$ is input electric phase delay the signal experiences in travelling from point 2 to the probe and $\alpha_r(x,y)$ is the reflected electric phase delay the signal experiences in travelling from the probe to point 2. For the case of a reciprocal circuit, $\alpha_i(x,y) = \alpha_r(x,y)$.

Because all loss terms outside of the DUT and the mixer conversion loss are frequency dependent, they must be calibrated from the measurements before an electric field magnitude at one frequency can be related to the electric field magnitude at another frequency. This is achieved through S-parameter measurements of the system and through mixer conversion loss measurements. The magnitude of the scattered electric field intercepted by the probe is given by: $E_s(x,y,z) \propto \sqrt{I^2 + Q^2}$

The final result from the amplitude measurements yield $E_{sr}(x,y,z) \propto L_r(x,y)\,A(x,y,z)$ for the reflected signal and $E_{st}(x,y,z) \propto L_t(x,y)\,A(x,y,z)$ for the transmitted signal.

Next, the net electrical phase delay at point (x,y) on the DUT can be determined by taking the inverse tangent of the I and Q channels. If a single moded region of constant phase is chosen as a reference point such as a cross section along a 50 Ω microstrip or coplanar waveguide transmission line at the input or output of the DUT, the phase delays due to the rest of the experiment can be subtracted from the argument of the signal. After such a calibration, we have the following electrical phase delay information for the reflected signal: $\alpha_i(x,y) + \alpha_r(x,y)$, and for the transmitted signal: $\alpha_i(x,y) + \alpha_t(x,y)$. If the device under test is reciprocal and linear then $\alpha_i(x,y) = \alpha_r(x,y)$.

Measurements

50 Ω Microstrip Transmission Line

At first, the validity of the experimental measurements are verified using a two inch long straight section of 50 Ω microstrip on RT/Duroid™ 5880 (ε_r=2.2, h=0.015"). A monopole probe is scanned over the same microstrip line with three different SMA terminations at 9 GHz (open, short, 50 Ω load). Figure 3a and figure 3b display the raw data collected from the in-phase signal and the quadrature signal of the 50 Ω microstrip with a matched load termination. Note how the peaks of the quadrature signal are spaced every 6500 μm. This corresponds exactly to a spacing of $\lambda_{eff}/4$ at 9 GHz. If the microstrip is lossless and reciprocal, and if the probe moves along a line parallel to the microstrip line, then $\alpha_i = \alpha_r$. The forms for the in-phase and quadrature signals from equation (1) reduce to:

$$I_r = B(x,y,z)\sin\left(\phi_o - 2\left(\frac{2\pi l}{\lambda_{eff}}\right)\right)$$
$$Q_r = B(x,y,z)\cos\left(\phi_o - 2\left(\frac{2\pi l}{\lambda_{eff}}\right)\right) \quad \text{(EQ 2)}$$

where the positionally invariant phases have been combined into the term ϕ_o, the positionally invariant losses and positionally varying reflected signal have been combined into the term $B(x,y,z)$, and the positionally varying phase term $(\alpha_i + \alpha_r) = 2(2\pi l/\lambda_{eff})$. The equations predict that the maxima and minima along a transmission line for the in-phase and quadrature signals are separated by a distance $\lambda_{eff}/4$ as can be seen from figure 3a and figure 3b.

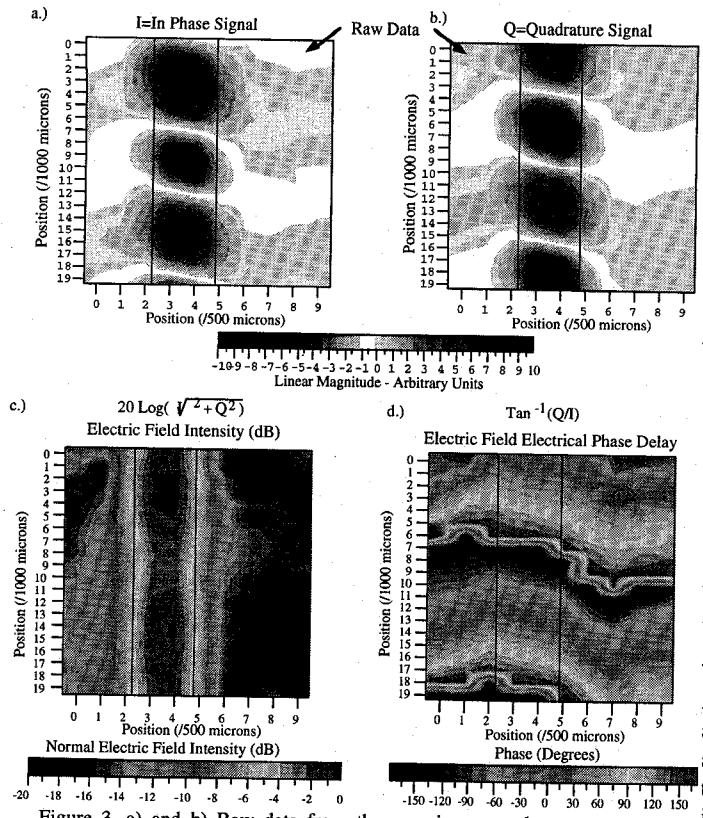

Figure 3. a) and b) Raw data from the experiment used to measure the normal electric field directly over a 50 Ω microstrip line fabricated on Roger's Corp. RT/Duroid (ε_r=2.2, w=1190 μm, and h=380 μm) at 9 GHz terminated with a 50 Ω load. c) Normal electric field intensity. d) Normal electric field phase delay

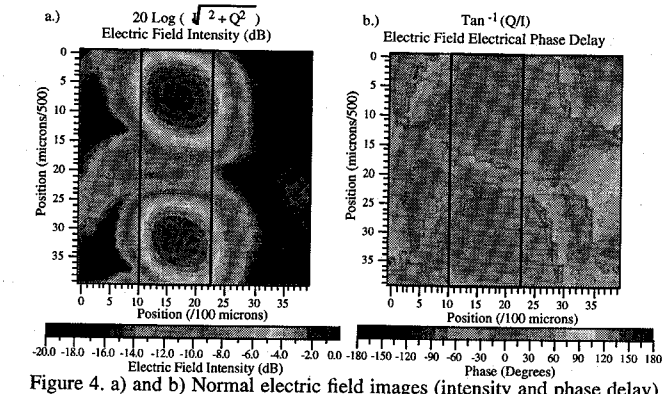

Figure 4. a) and b) Normal electric field images (intensity and phase delay) from a 50 Ω microstrip line fabricated on Roger's Corporation RT/Duroid (ε_r=2.2, width=1190 μm, and substrate height=380 μm) at 9 GHz terminated with an open.

The next step to validate the operation of the electric field imaging system is to combine the two signals (in-phase and quadrature) and examine the intensity of the normal electric field over the microstrip (Fig. 3c). It is seen that the intensities are nearly constant along contours parallel to the microstrip. An intensity ripple of 1.0 dB is present along the line which may be due to the non-ideal match of the termination or the non-ideal connections made with the SMA connectors at the input and output of the device.

The final validation is to check the phase variation of the signals along the microstrip line. The phase for a transmission line with a matched load will vary linearly with position and this is clearly seen from the measurements (Fig. 3d). The measured phase cycles by 2π every 13,000 μm which is $\lambda_{eff}/2$ as is predicted from transmission line theory. The slight angle in the phase is possibly due to a variation in the height of the probe across the microstrip.

Figure 4a displays the data collected from the same microstrip with an open at the end of the SMA connection at 9 GHz. As expected, the normal electric field intensity image in figure 4a yields standing waves with a -15 dB null in the center. The separation of the peaks is again 13,000 μm which is $\lambda_{eff}/2$. Figure 4b displays the electrical phase delay of each point over the microstrip and gives a zero phase response everywhere due to the presence of the standing waves.

Electric field intensity images of the microstrip with both shorted and open SMA terminations were compared with the same area. As predicted by transmission line theory, the nulls in the shorted microstrip occur at the peaks of the open microstrip and vice versa.

55 Ω Coplanar Waveguide Transmission Line

A coplanar waveguide (CPW) transmission line was fabricated and tested using Rogers Corporation RT/Duroid®, ε_r=10.8, and a dielectric thickness of 2,500 μm. The gap size is 255 μm and the center conductor width is 560 μm. Figure 5 displays three images of the measured normal electric field intensity over the coplanar waveguide line under different terminations (50 Ω load, open and short) at 2.3 GHz. In Figure 5a the normal electric field is nearly constant over contours parallel to the CPW line. Figure 5b shows the normal electric fields when the CPW line is terminated with an open. The presence of standing waves can clearly be seen with the nulls of the fields occurring at the top and bottom of the image. As was seen in the case of the microstrip, the peak of open CPW (Figure 5b) occurs in the same position as the null of the shorted CPW (Figure 5c).

Figure 6a-c) displays the tangential electric field intensity of the same CPW line as in figure 5a-c) with the same terminations (50 Ω load, open, and short). As expected, the tangential electric field is a minimum over the center conductor and is a maximum over the gaps of the CPW. The assymetry in the measurement is due to the interference of the monopole probe with the signal of the dipole probe. The monopole probe should be separated farther than 1 mm to minimize the interference with the dipole probe. It is expected that when the monopole and dipole probes are simultaneously in regions of strong normal and tangential electric fields that the coupling between the probes will yield undesirable results. This effect did not occur with the normal electric field images because the dipole was aligned parallel to the CPW line so that there were no strong tangential electric fields in the same direction as the center conductor line.

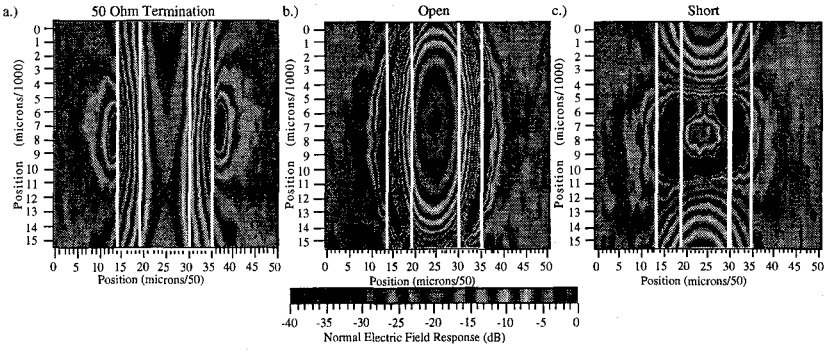

Figure 5. a) Normal electric field intensity over a 55 Ω CPW line. The CPW line is terminated with a 50 Ω SMA load. b) Same region as in a) but the CPW line is terminated with an open. c) Same region as in a) but the CPW line is terminated with an SMA short.

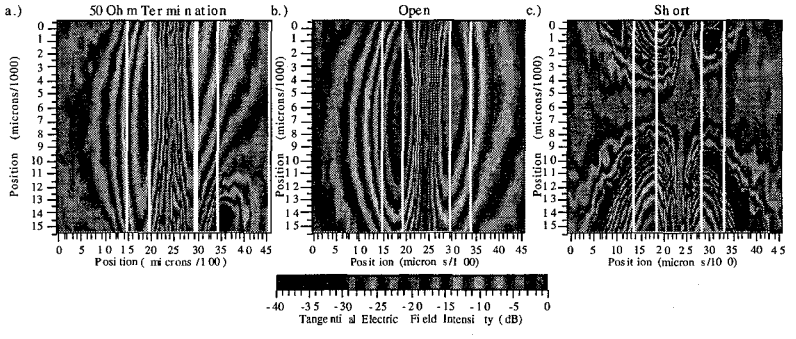

Figure 6. Tangential electric field intensity over a CPW line at 2.3 GHz. The line is terminated with a 50 Ω SMA load in a), an open in b) and a short in c).

Conclusions

In this paper we have presented an experimental electric field imaging system that uses the method of modulated scattering. The system improves upon the techniques used by Richmond [10] and Zürcher [13] by using very small probes (~100 μm long dipole and monopole arms) on thin quartz substrates with high frequency planar diodes. Furthermore, by using a system of circulators and absorptive RF switches the bandwidth and signal to noise ratio of the system is greatly improved. The probe design allows simultaneous measurements of the normal and tangential electric fields of the DUT. A simplified modulated scattering system theory has been presented and verified on a 50 Ω microstrip transmission line at 9 GHz and 55 Ω coplanar waveguide transmission line at 2.3 GHz.

Acknowledgments

The authors would like to thank Rogers Corporation for their generous donations of RT/duroid® substrates and Scott D. Waclawik for his help in assembling the electric field imaging system.

References

1. H. Cheng, J. F. Whitaker, "300 GHz Bandwidth Network Analysis Using Time-Domain Electro-Optic Sampling," 1993 IEEE MTT-S Digest, vol. 3, pp. 1355-1358.
2. W. Thomann, P. Russer, "Quasi-Simultaneous External Electro-Optic Probing of Transverse and Longitudinal Field Distributions taking into Account for Probe Tip Invasiveness," 1994 IEEE MTT-S Digest, Vol. 3, pp. 1601-1604.
3. J. Kim, J. Son, S. Wakana, J. Nees, S. Williamson, J. Whitaker, Y. Kwon, D. Pavlidis, "Time-Domain Network Analysis of MM-Wave Circuits Based on a Photoconductive Probe Sampling Technique," 1993 IEEE MTT-S Digest, Vol 3, pp. 1359-1362.
4. W. Mertin, C. Bohm, L. J. Balk, and E. Kubalek, "Two-dimensional field mapping of Amplitude and Phase of Microwave Fields inside a MMIC using the Direct Electro-Optic Technique," 1994 IEEE MTT-S Digest, vol. 3, pp. 1597-1600.
5. J. Bokor, A. M. Johnson, R. H. Storz, and W. M. Simpson, "High-Speed Circuit Measurements Using Photoemission Sampling," Applied Physics Letters, 49(4), July 28, 1986, pp. 226-228.
6. M. S. Hill, A. Gopinath, "Probing Gunn Domains at X-band Microwave Frequencies Using a Scanning Microscope," Journal of Physics D: Applied Physics, Vol. 7, 1974, pp. 69-77.
7. U. Mueller, C. Böhm, J. Sprengepiel, C. Roths, E. Kubalek and A. Beyer, "Geometrical and Voltage Resolution of Electrical Sampling Scanning Force Microscopy" IEEE MTT-S Digest, pp. 1605-1608, 1994.
8. C. Böhm, C. Roths, and E. Kubalek, "Contactless Electrical Characterization of MMICs by Device Internal Electrical Sampling Scanning-Force-Microscopy," IEEE MTT-S Digest, pp. 1605-1608, 1994.
9. Park Scientific Instruments, "PSI Probe," Technical Newsletter from PSI, Spring 1993.
10. J. H. Richmond, "A Modulated Scattering Technique for the Measurement of Field Distributions," Inst. Radio Eng. Trans. MTT-3, pp. 13-15, 1955.
11. A. L. Cullen, J. C. Parr, "A New Perturbation Method for Measuring Microwave Fields in Free Space," Proceedings IEE B 102, pp. 836-844, 1955.
12. R. Justice, V. H. Rumsey, "Measurement of Electric Field Distributions," Institute of Radio Eng. Transactions, AP-3, pp. 177-180, 1955.
13. J. Zürcher, "A Near Field Measurement Method Applied to Planar Structures," Microwave Engineering Europe, June/July 1992, pp. 43-51.
14. S. A. Bokhari, J. F. Zürcher, J. R. Mosig, F. E. Gardiol, "Near Fields of Microstrip Antennas," IEEE Transactions on Antennas and Propagation, 1994.
15. J. F. Nye, G. Hygate, "Measuring a microwave field close to a conductor," Measurement Science Technology 2 pp. 838-845, 1991.